J Solid State Electrochem (2009) 13:195–203
DOI 10.1007/s10008-008-0641-0

REVIEW

Surface chemistry and electronics of semiconductor–nanosystem junctions II: enzyme immobilization, charge transport aspects and scanning probe microscopy imaging

H. J. Lewerenz · K. Skorupska · J. R. Smith · S. A. Campbell

Received: 4 March 2008 / Revised: 25 July 2008 / Accepted: 29 July 2008 / Published online: 2 September 2008

Abstract Photoelectrochemically prepared and vapor-phase-induced surface nanotopographies are used for immobilization of enzymes at specific surface sites. The specific nanostructure of step-bunched silicon where the step edges are negatively charged and that of $MoTe_2$, characterized by negatively charged triangular growth defects, are successfully employed for enzyme immobilization. It is shown that, at pH values below the isoelectric point of the enzyme reverse transcriptase (RT), electrostatic interaction via the Debye length of 3–4 nm and the shorter ranged van der Waals attraction superimpose for enzyme adsorption at negatively charged surface sites. Scanning tunneling microscopy (STM) images of reverse transcriptases deposited onto the layered semiconductor $MoTe_2$ are interpreted in analogy to semiconductor–insulator–metal (MIS) device physics by analyzing the electronic properties of the junction between Pt tip (metal), biomolecule (insulator), and n-$MoTe_2$ (semiconductor). The uninhibited current flow in constant-current STM experiments is tentatively interpreted by salvation-assisted detrapping of electrons along the circumference of the proteins where biological water is present. Imaging of the RTs on step-bunched silicon surfaces with tapping mode atomic force microscopy shows spatially selective deposition at negatively charged step edges.

Keywords Protein · Immobilization · Semiconductor · Scanning probe microscopy · Charge transport

Contribution to the Fall Meeting of the European Materials Research Society, Symposium D: 9th International Symposium on Electrochemical/Chemical Reactivity of Metastable Materials, Warsaw, 17th–21st September, 2007

H. J. Lewerenz (✉) · K. Skorupska
Interface Engineering Group, Division of Solar Energy,
Hahn-Meitner-Institut,
Berlin, Germany
e-mail: lewerenz@hmi.de

J. R. Smith · S. A. Campbell
School of Pharmacy and Biomedical Sciences,
Portsmouth University,
Portsmouth, UK

Introduction

In this second part of research on semiconductor–nanosystem junctions, the original work is reviewed and, based on the inclusion of additional results and on advances in comprehension of the system, novel aspects have been added. Because of the complexity of the protein–semiconductor junction, several aspects are treated rather extensively to familiarize the reader with the relevant experimental and theoretical topics. Therefore, the Derjaguin, Landau, Verwey, and Overbeek (DLVO) theory and the Marcus–Gerischer theory for charge transfer at solid–electrolyte interfaces are shortly reviewed (see below), and also, the structure and functioning of the enzymes reverse transcriptase are described in some detail. Although only a first approximation, the electronic properties of the scanning tunneling microscopy (STM) metal tip–protein–semiconductor junction are analyzed on the basis of planar models for MOS or MIS (metal–oxide/insulator–semiconductor) structures.

The imaging of biological molecules and, in particular, of DNA by STM began shortly after the inception of the method [1, 2]. Most of the early work was done on conducting substrates such as highly-oriented pyrolitic graphite or Au [3, 4]. We were the first to use semiconducting substrates for imaging [5, 6]. The interpretation of the contrast of the images, recorded in the constant current mode, is difficult, particularly if the substrates are semiconducting or even insulating as in the

experiment of Guckenberger and co-workers [7, 8]. Immobilization of proteins has been an issue in bio-sensor development for a long time, and various approaches have been reported [9–11]. In our biomolecule–semiconductor system, we use (1) the defect nanostructure of the layered semiconductor $MoTe_2$, resulting from chemical vapor transport (CVT)-induced growth irregularities [12] and (2) the negatively charged step edges of so-called step-bunched Si surfaces [13, 14] as substrates for adsorption.

The proteins that are investigated in this study were selected due to their medical relevance and their unique, identifiable tertiary structure. Accordingly, the enzymes reverse transcriptase (RT) of the human immunodeficiency virus (HIV) 1, which is a heterodimeric protein with a well-known structure [15] and the RT of the avian myeloblastosis virus (AMV) have been chosen. Of particular interest is (1) the interaction between the enzymes and nanostructured surfaces with regard to their immobilization at specifically prepared sites and (2) the understanding of the imaging process. For the latter, we tentatively derive a model that explains the bias voltage dependence of the image contrast in STM. The model is based on analogies from semiconductor electronics and considers the STM-tip/protein/semiconductor junction energetics under different bias voltage conditions. Such analyses might be also useful in the development and advancement of so-called fourth generation solar cells, which combine inorganic and biological/organic entities.

Experimental

The HIV-1_{LAV} RTs were supplied from the Medical Research Council AIDS Reagent Project (National Institute for Biological Standards and Control, Potters Bar, Herts, UK). The handling of the reverse transcriptases involved dialyses and electrophoreses of the carrier solution as described in [16]. Scanning probe microscopy (SPM) experiments were performed in ambient air using (1) STM (Molecular Imaging) and (2) tapping mode atomic force microscopy (TM-AFM) (Nanoscope III, Digital Instruments). For STM, a Pt tip was used. Its apex was prepared by cutting a Pt wire with fine clippers. For TM-AFM, Si tips with curvature radii of $R<$ 10 nm (Veeco Instruments) were used. The experiments were done in ambient air. Substrate surfaces were obtained after CVT and cleaving of n-$MoTe_2$ to obtain fresh surfaces and by electrochemical conditioning of Si in alkaline electrolytes to obtain step-bunched surfaces. N-type (111) oriented samples with a doping concentration of 5×10^{14} cm^{-3} were used; the nominal miscut was 0°.

The deposition of biomolecules onto the surfaces was done using a syringe-type pipette. The enzymes with the carrier solution were deposited by droplet formation on the surface and left for ~1 h for evaporation of most of the carrier liquid. It should be noted that proteins are surrounded by the so-called biological water that is similarly strongly bound to the biomolecule surface as water films in Helmholtz layers at inorganic electrodes.

Results and discussion

Enzyme immobilization

Interaction forces between solution particles and surfaces are generally described by DLVO [17, 18], named after Derjarguin, Landau, Verwey, and Overbeek, and non-DLVO models [19, 20]. Originally developed for the description of colloidal stability, classical DLVO theory includes the interplay of electrostatic repulsion of equally charged colloids (where the electrostatic potential decreases inversely with distance showing $1/r$ behavior) and van der Waals attraction, which is short ranged ($1/r^6$). Particle–surface interactions are described by various additions to the original model, which include roughness, surface/interface chemistry, and steric hydration forces, for instance [21]. Accordingly, the topography and chemistry of substrate surfaces are strongly influential factors in biomolecule adsorption. Therefore, we first review the fundamental properties of the selected surfaces. Figure 1a shows a schematic of the structure of the layered semiconductor $MoTe_2$. In the trigonal prismatic arrangement of the $MoTe_2$ structure, saturated bonds form

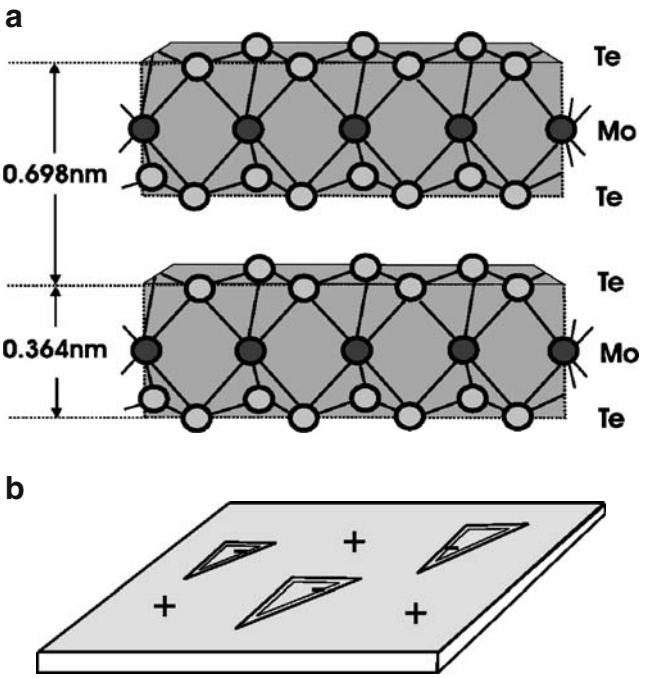

Fig. 1 Structural properties of $MoTe_2$; **a** sandwich structure and arrangement; **b** schematic of negatively charged triangular surface defects where surface states are formed at step edges

the outer surface of the individual sandwich layers. The material is characterized by a considerable density of triangular defects where reactive metal d-bonds are exposed to the ambient [22]. These sites are highly reactive, and negatively charged surface states are formed on n-type material. This results in a positive background charge and localized negative charge at the edges of the triangular defects as schematically shown in Fig. 1b. The size of these growth-induced defects ranges between 8 and 34 nm [23]. They are thus of similar size as the enzymes to be adsorbed [24]. Fresh and chemically rather inert surfaces can be prepared by mechanical cleaving of the layered material as already shortly mentioned above.

The second surface nanotopography, step-bunched Si, is prepared in alkaline electrolytes at cathodic potentials as shown in Fig. 1 of article I. The surface can also be chemically prepared [25], and a typical surface topographical AFM image can be seen in Fig. 2. The step edges are separated by extended atomic terraces and step heights vary in the range of 10–15 atomic bilayers (BL), which are 0.314 nm high. Synchrotron photoelectron spectroscopy (SRPES) and Kelvin probe microscopy (KPM) data [13] (Skorupska et al., to be published) show that step-bunched n-Si is in accumulation condition (the Fermi level at the surface is energetically closer to the conduction band than in the neutral bulk). In KPM experiments, it was found that negative charge accumulates near the step edges (Skorupska et al., to be published).

The heterodimeric enzymes RT have an isoelectric point (IP) at a pH of about 8.5–9 [26]. In the carrier solutions with pH close to that of physiological solutions (pH 7), the overall charge of the enzymes is positive. Therefore, providing surfaces with highly localized negative charge results in superimposed attractive electrostatic and van der Waals interaction at these sites. For the RT of HIV 1, a schematic of the tertiary/quaternary structure is presented in Fig. 3, where a ribbon representation has been chosen. It has become customary to compare this structure with that of the right human hand and label features accordingly as fingers, thumb, palm,

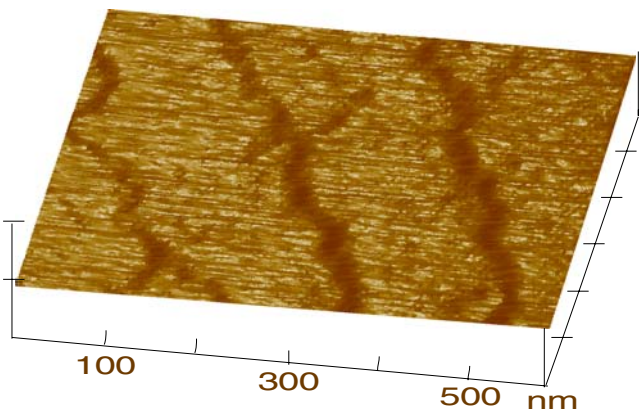

Fig. 2 AFM image of a step-bunched Si(111) surface (see text)

and connection. The larger subunit of 66 kDa comprises the RNase H, which has a cut-and-paste property in the complex process of reverse transcription [27].

To emphasize the medical relevance of this enzyme, we show an abbreviated schematic of the process of reverse transcription of the RT of HIV 1 in Fig. 4. The top graph of Fig. 4 shows the so-called minus strand synthesis, which sets in near the 5′ end of the original plus strand viral RNA where the transfer RNA (tRNA) acts as primer and binds to the primary binding site (PBS) of the host strand. The arrow indicates the growth direction of the new strand through the u5 region, ending at the r region of the viral genome. Below this graph, a further advanced situation of reverse transcription is depicted: the first jump (template exchange) of the synthesized minus strand genome has taken place after the Rnase H has digested the initial RNA host part (r, u5) but leaving the pbs unaffected. When the growing minus strand (see arrow) passes the polypurine tract (ppt) region of the template, the template escapes dissolution by Rnase H and itself serves as primer for plus strand synthesis by a mechanism called DNA-dependent DNA polymerization (DDDP) [28]. The third graph in Fig. 4 visualizes the situation where the template strand has largely been digested by Rnase H and minus strand synthesis of the first (lower) copied strand extends to the PBS site of the new strand, and the second strand, growing in the opposite direction, is almost completely synthesized. Only the original pbs and ppt sites remain. The arrows, labeled Rnase H, indicate the removal of tRNA and ppt. The then exposed PBS fuses with the PBS sequence at the 3′end of the minus-strand DNA, resulting in a circular DNA with overlapping 5′ends. The overall synthesis of the new proviral DNA strand is terminated at the template-strand breaks at the PBS and PPT ends, resulting in a linear molecule with long terminal repeats (not shown in the figure). The origin of the indicated nucleotide sequence gap is debated [29]. The strand discontinuity might constitute a binding site for a protein that mediates nuclear transport or integration of the provirus. In subsequent cell infection, the proviral DNA is spliced into the host genome, which results in synthesis of virus components. At that stage, the enzyme protease catalyzes the assembly of the viral parts. Antiviral drug therapy uses reverse transcriptase and protease inhibitors as well as fusion inhibitors [30] to avoid entering of the virus into a cell.

SPM imaging

Figure 5 shows an STM image of an RT of HIV 1 on $MoTe_2$. The heterodimer structure with the two subunits, the connection area and the central hole with the polymerase active site, are clearly discernible. The height of the molecule is about 2 nm, and its lateral dimensions are about 7 nm for the short and 24 nm for the long section through

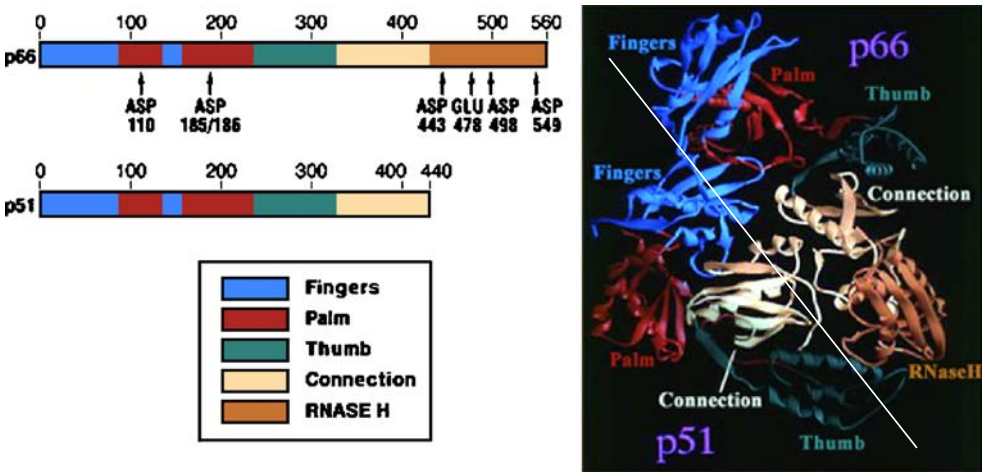

Fig. 3 Ribbon representation of the tertiary/quaternary structure of the reverse transcriptase of HIV 1 showing the two subdomains with atomic weight 66 and 51 kDa and labeling of the substructures according to the human right hand with thumb, palm, and fingers as roughly indicated by the *white line*; the RNase H domain of the 66 kDa subunit and the connection are shown. Also indicated are amino acid sequences such as asp and glu; the 66 kDa subunit is 560 amino acids long and the 51 kDa contains the first 440 amino acids of the p66 subunit

the molecule. In Figs. 6 and 7, hybrids of RT and synthesized proviral DNA are displayed. For this and the subsequent image, rather involved incubation experiments have been performed in order to "catch" the situation were synthesis becomes visible: If the incubation time for strand synthesis exceeds a rather narrow time interval, the RTs detach from the strand, whereas for a too short incubation time, synthesis has not yet become visible. Details of the experiment are given in [16]. The images show the first STM images of RTs attached to synthesized DNA strands. In Fig. 8, an AMV RT enzyme, deposited onto a step-bunched Si surface and imaged by TM-AFM shows that the substructure of the RT can also be imaged by this currentless method. The immobilization situation is similar to that on $MoTe_2$ because here, too, the positively charged protein adsorbs at negatively charged sites at the step edges. In addi-

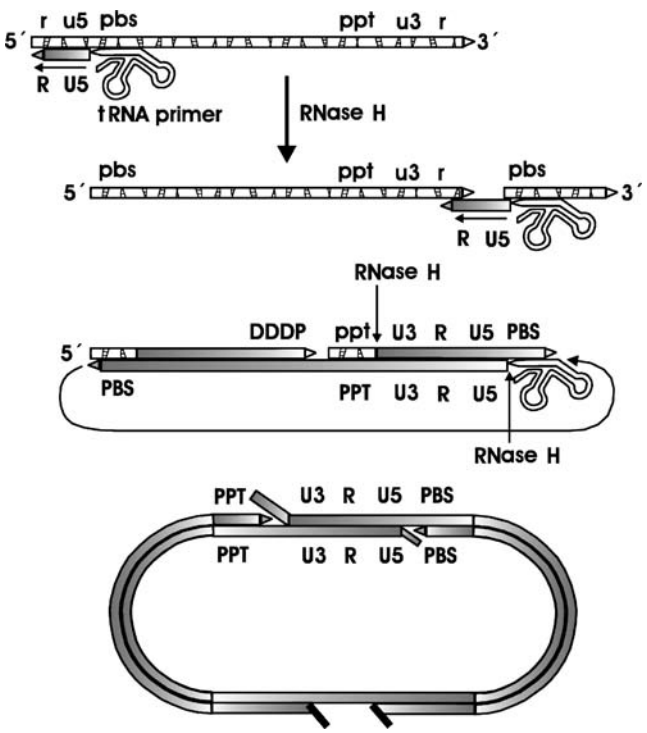

Fig. 4 Shortened version of the process of reverse transcription to four steps; the last step, the linearization of the circular structure, is not included.Tthe original viral RNA strand is shown as *structured white strand*; the synthesized minus and plus strands are in *gray-white tone*. *Small lettering* refers to the subunits of the original RNA strand, *large letters* to the synthesized proviral strands. *ppt*, *PPT* Polypurine tracts; *pbs*, *PBS* primer binding sites; *tRNA* transfer RNA pimer; *DDDP* DNA-dependent DNA polymerization (see text)

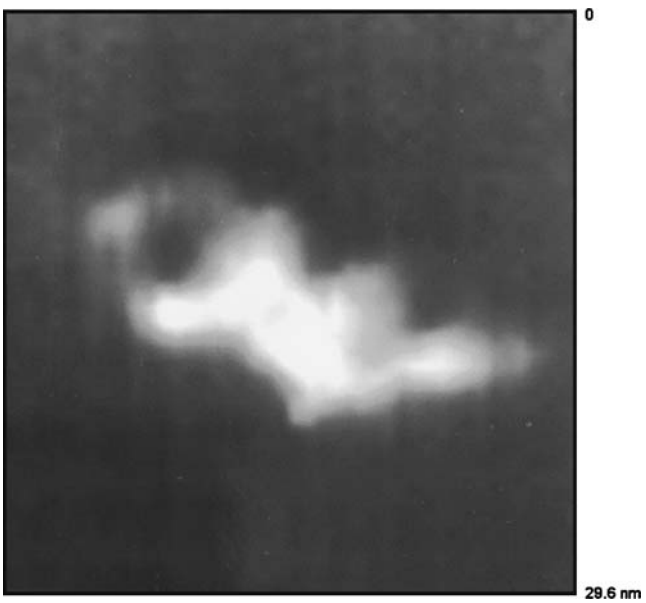

Fig. 5 STM image of an RT of HIV 1, deposited onto n-$MoTe_2$; V= −0.7 V ($MoTe_2$ vs. Pt tip) recorded in ambient air

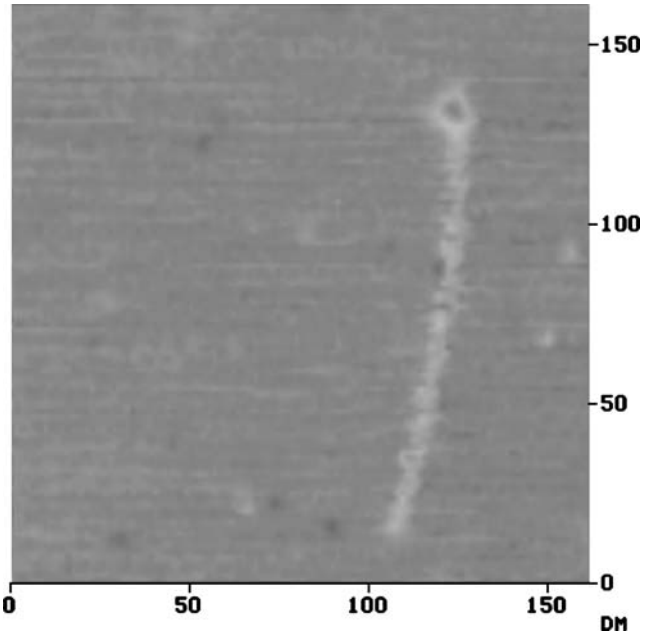

Fig. 6 STM image of an RT-DNA hybrid of the avian myeloblastosis virus (*AMV*); conditions as in Fig. 5

tion, at these sites, the electric field strength is increased due to the non-planar geometry. Such interactions belong to the so-called non-DLVO class [19, 20].

Junction electronics: a working hypothesis

The mechanism of STM imaging of biological molecules has not yet been unambigously identified. A well-known unsolved example is provided by the experiments of Guckenberger et al. [7, 8] who imaged DNA on insulating mica at rather high bias voltage between tip and substrate at increased relative humidity levels. A typical result is shown in Fig. 9. The "ultrahigh conductivity of ultrathin water films" postulated in the interpretation of these experiments remained yet unexplained and explanations invoking an alternative, i.e., electrochemical, charge transport mechanism had been advocated [31]. Hitherto, theories for charge transfer across biological molecules [32–34] do not include electrostatic fields across the biomolecule. The existing models consider tunneling, hopping, and super-exchange charge transfer/transport processes [35, 36]. It is presently not clear whether and to which extent these processes contribute to the contrast

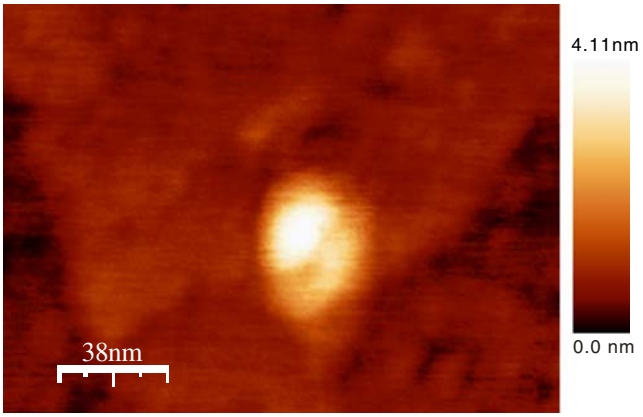

Fig. 8 TM-AFM image of the AMV RT deposited onto a step bunched Si(111) surface with a typical zigzag surface topography. Adsorption near the re-entry site at a step edge is visible

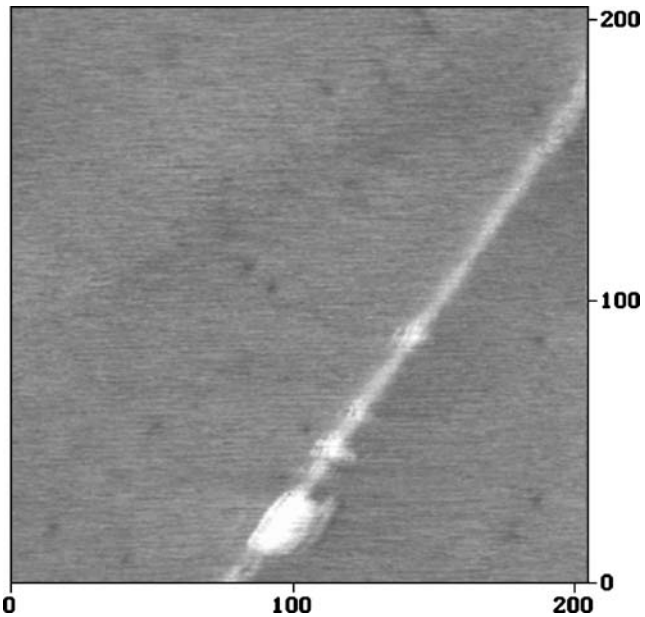

Fig. 7 STM image of molecular chain and C-shaped entity of AMV-RT hybrid; conditions as in Fig. 5

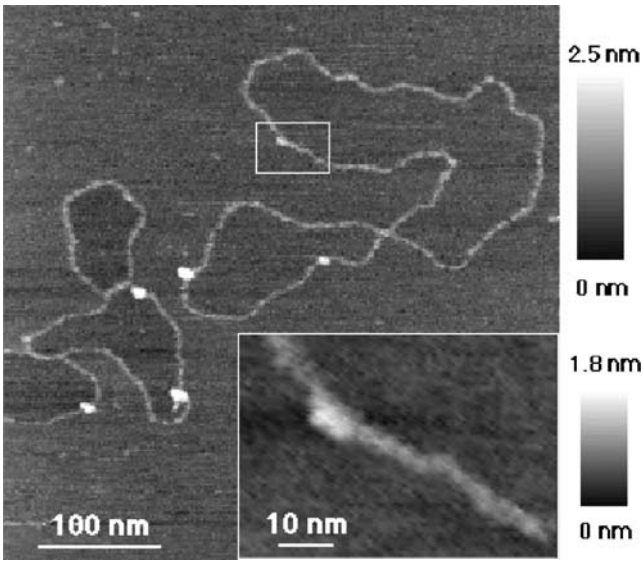

Fig. 9 Plasmid DNA on mica imaged with STM in humid air (data from the homepage of the Max-Planck-Institute in Martinsried); typical parameters, V ~7 V vs. grounded tip; tunneling current I_T ≤1pA; relative humidity ~70% (see text)

observed in constant current STM experiments. We first summarize our findings and comment on them:

1. The high resolution and contrast of the images indicate that imaging was not limited by electrical resistance across the various subunits of the enzyme; otherwise, a region of low conductivity would induce the approach of the STM tip with subsequent penetration of the molecule and its disruption. We have observed such behavior in other experiments at somewhat increased bias voltages [5].
2. The substructure of the images in Figs. 5, 6, 7, 8, and 9 is very well resolved. In ribbon-type presentations of the RTs (Fig. 3), strong spatial variations of the polypeptide chains within the protein exist, which makes it difficult to assume a spatially homogeneous and highly effective charge transport mechanism (such as a combination of interchain tunneling and hopping along chains) through the molecule that results in electron transfer to the STM tip.
3. STM imaging of the molecules occurred at bias voltages of −0.7 V for 200pA constant current but not below this value. This finding points to specific junction electronics at the Pt-tip/protein/n-type semiconductor contact.

For discussion, we review the experimental situation in Fig. 10 where the overall experimental geometry, including the electric field from semiconductor to STM tip, is shown at contact, without external bias. It should be kept in mind that STM imaging occurred at a bias of −0.7 V of $MoTe_2$ vs. the grounded tip. This situation will be further analyzed in this paper. Because of the doping range of $MoTe_2$ in the range of 10^{17} cm^{-3}, a space charge layer of ~100 nm extension exists and the corresponding equipotential lines of this layer are indicated as semicircles in the figure. At −0.7-V bias, the situation is inversed: The semiconductor is more negative than the tip. The electric field points from the tip toward the semiconductor, with the protein and the air gap between them, as shown in Fig. 11b. Also shown in Fig. 11b is the valence band density of states, measured by ultraviolet photoelectron spectroscopy (UPS) and a process is indicated where electrons from the valence band tunnel into the empty states of the tip via transport across the biomolecule (see below).

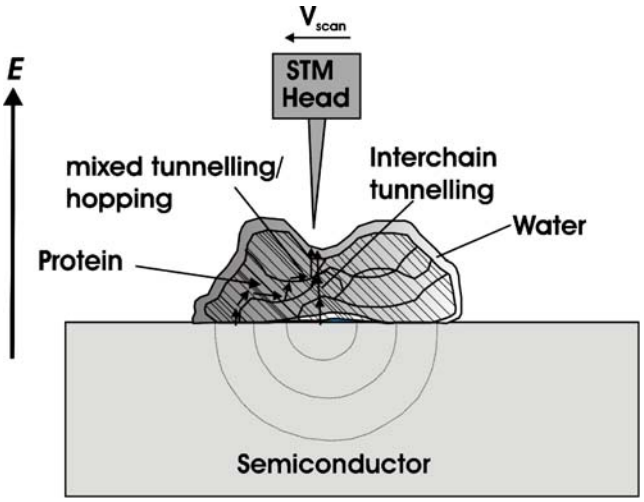

Fig. 10 Schematic of the STM experiment showing possible charge transport routes as indicated (see also text)

In the following, the junction analysis is based on the concepts of applied semiconductor physics (see also the "Discussion" of article I). The electronic properties of the junction are described by the potential distribution across it, as typically done for MOS or MIS (metal–insulator–semiconductor) structures. Presently, there is no reason to assume that these concepts can not be transferred to junctions that include

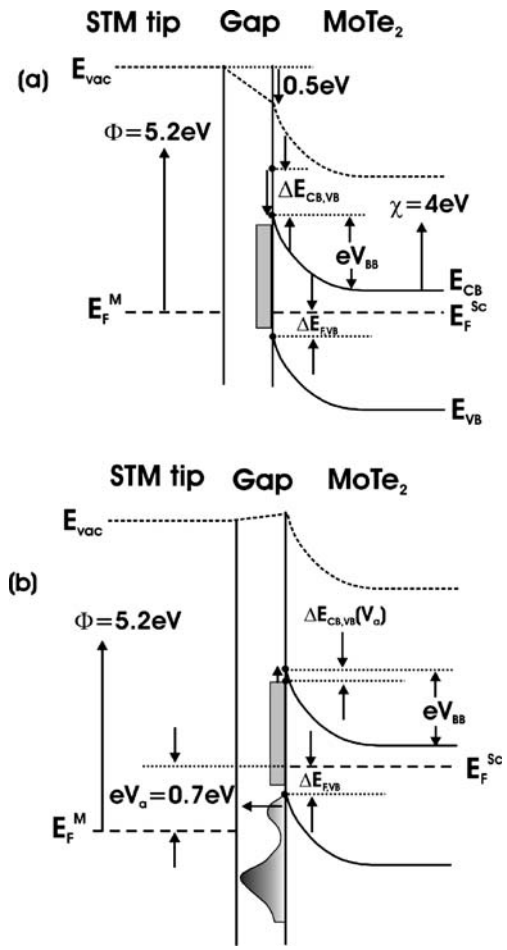

Fig. 11 Energy diagram of the situation at the STM tip–enzyme–semiconductor contact; the *shaded area* indicates negatively charged semiconductor surface states. A surface state induced band bending of n-$MoTe_2$ of ~0.5 eV has been assumed. χ Semiconductor electron affinity; E_F^M tip Fermi level; E_F^{SC} semiconductor Fermi level; E_{Vac} vacuum level; $\Delta E_{CB,VB}$ band-edge shift due to Fermi level pinning; eV_a semiconductor Fermi level shift due to applied voltage V_a; $\Delta E_{F,VB}$ energetic distance between Fermi level at the surface and the valence band edge. **a** Junction in contact, **b** junction at a forward bias of −0.7 V; note the inversion of the electrostatic potential (E_{Vac}) across the biomolecule compared to the situation in Fig. 11a

biological molecules, particularly when considering that analogous concepts are used at the solid-electrolyte phase boundary and in bioelectrochemistry. In Fig. 11a, the energy vs. space diagram depicts the electronic situation at contact between n-$MoTe_2$ and the Pt tip of the STM. Because of the narrow tip curvature, the Pt work function Φ has been assumed to be lower than the bulk value of ~5.7 eV. We take 5.2 eV for Φ. Presently, the correct value cannot be determined, and we stress here that the discussion that follows is tentative. It will be shown, however, that we are able to explain the image process semiquantitatively. The electron affinity of $MoTe_2$ has been measured by UPS where the extrapolation of the secondary electron cut-off gives a value close to 4 eV [6]. The energy gap of the semiconductor was determined by optical measurements, yielding 1.0–1.1 eV. The contact potential (energy) difference is then given by the work function difference between the Pt tip and the semiconductor Fermi level. Assuming a typical value of 0.2 eV for the energetic distance between conduction band and Fermi level, the work function of n-$MoTe_2$ is 4.2 eV, resulting in a difference in the Fermi level position before contact of $\Delta\Phi$= 1 eV. Because of the large number of defects on the surface of $MoTe_2$, strong Fermi level pinning is assumed. The latter is characterized by the independence of the barrier height on the contact potential or on the work function of the contacting metal in Schottky junctions or at redox electrolyte–semiconductor contacts [36]. A band bending eV_{BB} due to surface states has been assumed where the semiconductor Fermi level is close to the valence band maximum without reaching the strong inversion condition for which $E_F^S - E_{VB} \leq$ 0.2–0.3 eV (E_F^S denotes the energetic position of the Fermi level at the surface). The surface states in Fig. 11 are indicated by a gray box at the surface. With ~0.5 eV band bending, the remaining contact potential difference drops across the interfacial layer with the biomolecule in it. The band-edge shift is indicated by a downward-oriented arrow at the semiconductor surface. This shift of 0.5 eV is also seen in the Galvani potential (vacuum level, E_{Vac}) of the junction.

Under forward bias of −0.7 V (Fig. 11b) of the semiconductor vs. grounded tip, the high-surface state density and the resulting strong Fermi level pinning [22] lead to an upward shift of the semiconductor band edges without change in band bending (small upwards arrow in Fig. 11b). This inverts the direction of the electric field across the junction, and electrons can be transferred from the semiconductor valence band to the tip through or across the interlayer with the protein as indicated by the horizontal arrow in the figure. The possibility that tunneling occurs via occupied surface states into empty states of the tip cannot be excluded because the density of surface states (in the range of $>10^{13}$ cm^{-2} eV^{-1}) and the high density of d-band bulk states of the material (~10^{20} cm^{-3} eV^{-1}, see UPS data) are not too dissimilar. In future work, the surface DOS will be investigated by capacitance analysis to determine its energetic distribution.

Charge transfer aspects

Considerations on the charge transfer mechanism that describes the observed behavior are also based on observations of Guckenberger et al. [7, 8] (Fig. 9): In their pA STM experiments, currents were observed on insulating mica that allowed imaging of insulating polypeptides such as DNA under a forward bias of ~7 V vs. tip. Imaging was dependent on relative humidity (RH) levels with contrast obtained at RH ~70%. The origin of the noted conductivity increase of surface water by a factor of 10^4–10^5 compared to bulk water has been debated. Whereas Guckenberger et al. maintain that the image contrast results from tunneling, Fan and Bard [31] proposed an electrolytic conduction mechanism along the ultrathin surface water film.

In the formulation of our transport hypothesis, first, the variation of the electron potential energy along polypeptides of about $V_{el} \leq 0.6$ eV [37] is considered. At room temperature, the electron release time from the trap by thermal activation would be in the order of seconds, i.e., much too slow for efficient charge transport. In the presence of water (moisture), localized electrons will be hydrated and a solvation shell will be formed. Electron solvation is an ultrafast process occurring in the time range 50 fs–2 ps [38, 39]. The

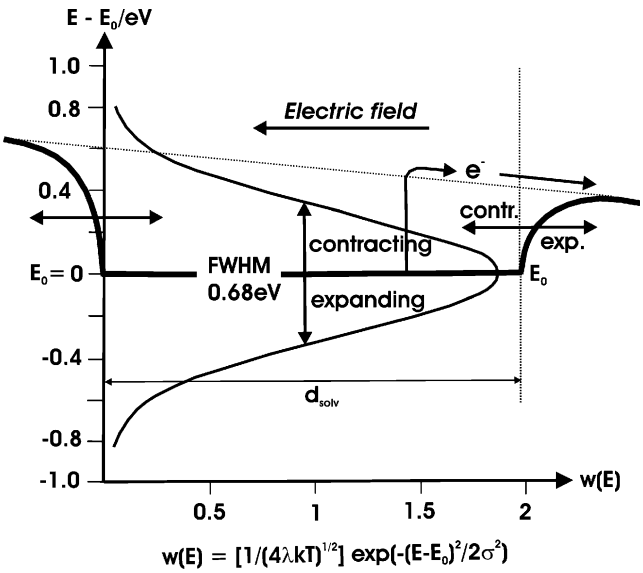

Fig. 12 Schematic of the solvation cage for an electron at a trap site on polypeptide chains; although the water will not be able to move freely as for electrons injected into water, the data were taken for that situation to show the principle of solvation-assisted electron release from traps; $w(E)$ Marcus–Gerischer probability for collective electron excitation, λ solvent reorganization energy, E_m energetic position of the electron at the trap site, E static electric field along the polypeptide chain due to the properties of the semiconductor–protein–STM metal tip junction

reorganization energy of free electrons in water is 1.6 eV [40]. Although not fully appropriate due to the localization of the electron on the polypeptide backbone, we take this value for a first approximation. This solvent reorganization energy λ translates into an electron energy increase according to the Marcus–Gerischer theory [41, 42]. The free energy increase for electrons in water yields a value of 0.34 eV in the contracting mode of the solvation shell. Hence, this concept is advocated in this paper to emphasize the possibility of collective hydration-induced thermal excitation of electrons from trap sites that occurs at room temperature and that is ultrafast. Figure 12 shows a schematic of electron release from an asymmetrically deformed trap site using Marcus–Gerischer theory. The electric field strength across the enzyme is larger than 10^5 V cm^{-1}, even without considering its increase due to the tip curvature, and thus could deform the atomic potentials along the polypeptide chain, providing directed charge transport toward the tip. The ribbon structure in Fig. 3 indicates that electron transport across the molecule would involve interchain tunneling and hopping along chains, which should show spatial differences in conductivity of the molecule that is not seen at 200 pA constant current. Therefore, we propose that the charge transport is based on

1. Transport at the outer surface of the protein (see Fig. 10) where the so-called biological water provides the possibility for solvation assisted hopping and
2. The fact that resonant injection of electrons into the enzyme extended LUMO orbitals occurs from the valence band or high density surface states [43].

Attachment of biological water to the protein is comparably strong, similar to that of water in Helmholtz layers [44] at metal electrodes. This is likely the reason for its presence under the ambient imaging conditions of our experiments. The proposed mechanism explains the high conductivity observed in our experiments, the bias voltage dependence of the image contrast, and the conductive properties of the so-called surface water in the Guckenberger experiments on mica.

Conclusions

Based on the ultrahigh resolution of enzymes with STM, performed in ambient air, we developed a working hypothesis of a resonant charge injection mechanism and analyze the junction energetics at the STM-tip/protein/semiconductor contact using the concepts of applied semiconductor physics for MOS or MIS junctions. The bias dependence of the image contrast can be explained assuming strong Fermi level pinning of the defect-rich $MoTe_2$ substrate. For subsequent electron transport, we propose that a type of hopping mechanism is active at room temperature where electrons are released from trap sites at the polypeptide by ultrafast solvation excitation. This mechanism would also explain the hitherto unexplained observations of Guckenberger et al. where STM imaging occurred on insulating mica at elevated humidity levels.

References

1. Engel A (1991) Annu Rev Biophys Biophys Chem 20:79 doi:10.1146/annurev.bb.20.060191.000455
2. Baro AM, Miranda R, Alaman J, Garcia N, Binig G et al (1985) Nature 315:253 doi:10.1038/315253a0
3. Miles MJ, Carr HJ, McMaster TC, Tatham AS et al (1991) Proc Natl Acad Sci U S A 88:68 doi:10.1073/pnas.88.1.68
4. Lindsay S, Thundat T, Nagahara L, Knipping U, Rill R (1989) Science 244:1063 doi:10.1126/science.2727694
5. Lewerenz HJ, Jungblut H, Campbell SA, Müller DJ (1992) AIDS Res Hum Retrovir 8:1663
6. Jungblut H, Campbell SA, Giersig M, Müller DJ, Lewerenz HJ (1992) Faraday Discuss 94:183 doi:10.1039/fd9929400183
7. Guckenberger R, Heim M, Cevc G, Knapp HF, Wiegrabe W, Hillebrand A (1994) Science 266:1538
8. Heim M, Steigerwald M, Guckenberger R (1997) J Struct Biol 119:212
9. Yin F, Shin H-Kand Kwon Y-S (2005) Biosens Bioelectron 21:21 doi:10.1016/j.bios.2005.04.014
10. Neves-Petersen MT, Snabe T, Klitgaard S, Duroux M, Petersen SB (2005) SB. Protein Sci 15:343 doi:10.1110/ps.051885306
11. Boozer C, Ladd J, Chen S, Jiang S (2006) Anal Chem 78:1515 doi:10.1021/ac051923l
12. Conan A, Bonnet A, Arnrouche A, Spiesser M (1984) J Phys Fr 45:459 doi:10.1051/jphys:01984004503045900
13. Skorupska K, Lublow M, Kanis M, Jungblut H, Lewerenz HJ (2005) Appl Phys Lett 87:262101 doi:10.1063/1.2150267
14. Skorupska K, Lublow M, Kanis M, Jungblut H, Lewerenz HJ (2005) Electrochem Commun 7:1077 doi:10.1016/j.elecom.2005.07.012
15. Kohlstaedt LA, Wang J, Friedman JM, Rice PA, Steitz TA (1992) Science 256:1783 doi:10.1126/science.1377403
16. Campbell SA, Smith JR, Jungblut H, Lewerenz HJ (2007) J Electroanal Chem 599:313 doi:10.1016/j.jelechem.2006.05.035
17. Derjarguin BV, Landau L (1941) Acta Physico-Chimica 14:633 (URSS)
18. Verwey EJ, Overbeek JTG (1948) Theory of the stability of lyophobic colloids. Elsevier, Amsterdam
19. Grasso D, Subramanian K, Butkus M, Strevett K, Bergendahl J (2002) Rev Environ Sci Biotechnol 1:17 doi:10.1023/A:1015146710500
20. Petsev DN, Vekilov PG (2000) Phys Rev Lett 84:1339 doi:10.1103/PhysRevLett.84.1339
21. Israelachvili JN (1992) Intermolecular and surface forces. Academic, London
22. Lewerenz HJ, Gerischer H, Lübke M (1984) J Electrochem Soc 131:100 doi:10.1149/1.2115467
23. Skorupska K, Smith JR, Campbell SA, Jungblut H, Lewerenz HJ (2007) ECS Trans 2:63 doi:10.1149/1.2409009
24. Jacobo-Molina A, Ding J, Nanni RG, Clark AD, Lu X Jr, Tantillo C et al (1993) Proc Natl Acad Sci U S A 90:6320 doi:10.1073/pnas.90.13.6320
25. Garcia S, Bao H, Hines MA (2004) Phys Rev Lett 93:166102 doi:10.1103/PhysRevLett.93.166102

26. Müller B, Restle T, Kühnel H, Goody RS (1991) J Biol Chem 266:14709
27. Starnes MC, Cheng YC (1989) J Biol Chem 264:7073
28. Skasko M, Weiss KK, Reynolds HM, Jamburuthugoda V, Lee K, Kim B (2005) J Biol Chem 280:12190 doi:10.1074/jbc.M412859200
29. Charneau P, Clavel F (1991) J Virol 65:2415
30. Rocksroh JK, Mauss S (2004) J Antimicrob Chemother 53:700 doi:10.1093/jac/dkh161
31. Fan FRF, Bard AJ (1995) Science 270:1849 doi:10.1126/science.270.5243.1849
32. Marcus RA (1965) J Chem Phys 43:679 doi:10.1063/1.1696792
33. Rosokha SV, Newton MD, Head-Gordon M, Kochi JK (2006) CPPC 324:117
34. Cave RJ, Newton MD (1997) J Chem Phys 106:9213 doi:10.1063/1.474023
35. Giese B (2000) Acc Chem Res 33:631 doi:10.1021/ar990040b
36. Lewerenz HJ (1993) J Electroanal Chem 356:121 doi:10.1016/0022-0728(93)80515-J
37. Schlag EW, Sheu S-Y, Yang D-Y, Selzle HL, Lin SH (2000) Proc Natl Acad Sci U S A 97:1068 doi:10.1073/pnas.97.3.1068
38. Kambhampati P, Son DH, Kee TW, Barbara PF (2002) J Phys Chem A 106:2374 doi:10.1021/jp014291p
39. Paik DH, Lee IR, Yang D-S, Baskin JS, Zewail AH (2004) Science 306:672 doi:10.1126/science.1102827
40. Coe JV, Earhart AD, Cohen MH, Hoffman GJ, Sarkas HW, Bowen KH (1997) J Phys Chem 107:6023 doi:10.1063/1.474271
41. Gerischer H (1960) Z Phys Chem NF 6:223
42. Gerischer H (1961) Z Phys Chem NF 26:40
43. Lewerenz HJ (2008) Phys Status Solidi (in press)
44. v Helmholtz H (1879) Wiedemanns. Ann Phys 7:337